IEEE Access
Multidisciplinary | Rapid Review | Open Access Journal

Received Date December 12, 2016; accepted December 26, 2016, date of publication December 29, 2016, date of current version January 27, 2017.

Digital Object Identifier 10.1109/ACCESS.2016.2645938

SIW Butler Matrix with Modified Hybrid Coupler for Slot Antenna Array

QING-LING YANG[1], YONG-LING BAN[1], JI-WEI LIAN[1], ZHE-FENG YU[2], AND BIAN WU[3]

[1]School of Electronic Engineering, University of Electronic Science and Technology of China, Chengdu 611731, China
[2]China Aerodynamics Research and Development Center, Mianyang 621000, China
[3]School of Electronic Engineering, Xidian University, Xi'an 710126, China

Corresponding author: Y.-L. Ban (byl@uestc.edu.cn)

This work was supported in part by the National Natural Science Foundation of China under Grant 6147109 and in part by the Mainland-Hong Kong-Macau-Taiwan Science and Technology Cooperation Project under Grant 2015DFT10170.

ABSTRACT This paper presents a substrate integrated waveguide Butler matrix with a modified hybrid coupler, operating from 28 to 32 GHz. The modified hybrid coupler is realized by using 90° hybrid coupler followed by a −45° compensating phase shifter. Thus, 45°/135° output phase differences can be obtained using this type of coupler. Compared with the equal-length unequal-width phase shifter, the compensating phase shifter exhibits better phase characteristics, with only 3° phase error over 28–32 GHz. Because the phase of compensating phase shifter is not realized by taking the phase introduced by the crossover as a reference, it gives great flexibility to the design of compensating phase shifter. Adopting the modified hybrid coupler, the designed Butler matrix features the output phases with peak to peak error of 13° and wideband performance from 28 to 32 GHz. The slot array fed by the Butler matrix can radiate four slanted beams with acceptable measured gains, in the range of 9.7∼12 dBi for port 1 excitation and 8.4∼11.1 dBi for port 2 excitation. The radiated beams can reach a wide azimuthal coverage between ±61°.

INDEX TERMS Modified hybrid coupler, Butler matrix, compensating phase shifter, slot array antenna, substrate integrated waveguide (SIW).

I. INTRODUCTION

Multibeam antenna arrays with passive beamforming networks (BFN) [1]–[7] are potential candidates for 5G millimetre-wave (mmWave) wireless communications. This is because of their simple structure, low cost and low power dissipation. As a practical BFN, the Butler matrix with simple configuration and wide bandwidth has been usually chosen as multibeam feeding network. A number of studies on Butler matrix have been carried out [5], [8]–[11], such as the miniaturization of Butler matrix in [8] and [9] and two-dimensional beam scanning to obtain wider coverage area in [5] and [10].

Essentially, a Butler matrix [2], [12] is a device that can provide power dividing and required output phase shifting. It usually consists of hybrid couplers, phase shifters and crossovers, as shown in Fig. 1. As different input ports are excited, four output signals will be produced with uniform amplitudes and adjacent output ports will exhibit uniform phase differences. The output phase differences varying with input ports are tabulated in Table I. Antenna arrays fed by Butler matrix are capable of radiating four beams in various directions. In conventional Butler matrix, the phase of 135° phase shifter is realized by taking the phase introduced by the crossover [6]. However, once it is designed, the phase of crossover is fixed, which will restrict the design flexibility of 135° phase shifter. Consequently, to design a phase shifter with good performance is usually difficult and intricate. To address these issues and facilitate the designs, one method that is considered to be practical and helpful has been reported in [2] and [13]. They all omit the design of crossover and have advantages of simpler architecture and better phase balance compared with the traditional Butler matrix. However, the disadvantage is that they occupy a larger area. Furthermore, the feedings of these structures are distributed across two different locations. In some cases such as mobile terminals, it is better to arrange the feeding ports to one side and antenna array to the clearance area [14]. Therefore, in this regard, this structure is not applicable to these scenarios.

Given the above-mentioned issues, a SIW Butler matrix with modified hybrid coupler is proposed. For this structure, the 135° phase shifter is incorporated into the design of

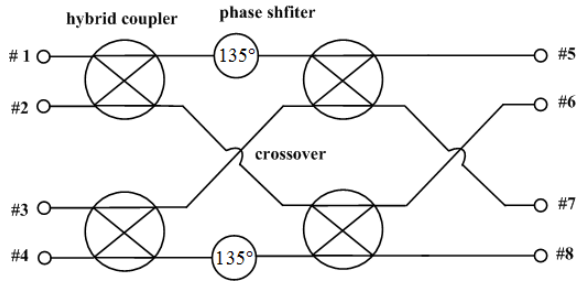

FIGURE 1. Topology of the conventional Butler matrix.

TABLE 1. Relationships between feedings and output phase differences.

Feeding port	port 1	port 2	port 3	port 4
Output phase difference	–45°	135°	–135°	45°

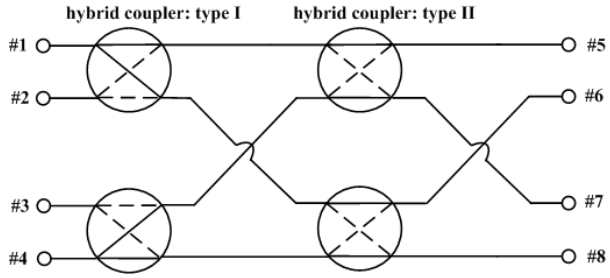

FIGURE 2. Topology of the proposed Butler matrix.

hybrid coupler. Therefore, the original 135° phase shifting can be accomplished by this modified hybrid coupler. Since the phase of 135° phase shifter does not take the crossover as a reference, it is obvious that the overall design will be more agile and efficient. Similar SIW directional couplers with 180° output phase difference are reported in [15] and [16], which are realized by combining the hybrid coupler with a 90° phase shifter.

This paper is organized as follows. The detailed design theory and considerations are presented in Section II. The design procedures of Butler matrix are illustrated in Section III. Section IV discusses the slot array antenna design, physical fabrication and measured results of the multibeam array. At last, the concluding remarks are given in Section V.

II. THEORY AND DESIGN

The topology of the proposed Butler matrix is shown in Fig. 2. In this structure, two types of hybrid coupler are included. To facilitate the analysis, they are temporarily referred to as type I and type II hybrid coupler. The output phase differences of type I hybrid coupler are assumed to be φ_{23} when port 1 is fed, and φ_{32} when port 4 is fed. In addition, φ_{23} is characterized by $\mathrm{Ang}(S_{21}) - \mathrm{Ang}(S_{31})$, and φ_{32} by $\mathrm{Ang}(S_{34}) - \mathrm{Ang}(S_{24})$. Similarly, for type II hybrid coupler, its output phase differences are assumed to be θ_{23} when port 1 is fed andθ_{32} when port 4 is fed. θ_{23} is characterized by

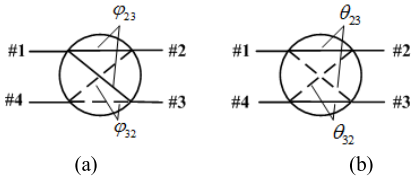

FIGURE 3. Diagram of output phase differences. (a) type I hybrid coupler; (2) type II hybrid coupler.

$\mathrm{Ang}(S_{21}) - \mathrm{Ang}(S_{31})$ and θ_{32} by $\mathrm{Ang}(S_{34}) - \mathrm{Ang}(S_{24})$. They can be figuratively seen in Fig. 3. To illuminate the signal meandering paths when port 1 and port 2 are fed, significant locations are labelled with capital letters, shown in Fig. 4. With port 1 excitation, the wave meandering to port 5 $\sim$ 8 follows the paths: $A \to C \to E \to G \to K$, $A \to D \to F \to I \to L$, $A \to C \to E \to H \to M$ and $A \to D \to F \to J \to N$, respectively. Each meandering travels through two hybrid couplers.

Because the 135° phase shifter is incorporated into the hybrid coupler, the phase differences between two adjacent output ports completely originate from the output phase differences of two types of hybrid couplers. Therefore, for wave meandering to port 5 and port 6, the output phase differences can be obtained from the phase difference between path AD and AC (namely $-\varphi_{23}$) and phase difference between path FI and EG (namely 0°), so the total output phase difference between port 6 and port 5 can be described as $-\varphi_{23} + 0 = -\varphi_{23}$. In the same manner, the output phase differences between port 7 and port 6, port 8 and port 7 equal $\varphi_{23} - \theta_{23}$ and $-\varphi_{23}$, respectively. From Table I we can learn that the phase differences of two adjacent output ports are $-45°$ for port 1 excitation. Hence, the above relationships can be expressed by the following equations

$$\begin{cases} -\varphi_{23} = -45° \\ \varphi_{23} - \theta_{23} = -45° \end{cases} \tag{1}$$

In comparison, for port 2 excitation, wave travelling to port 5 $\sim$ 8 follows the path: $B \to C \to E \to G \to K$, $B \to D \to F \to I \to L$, $B \to C \to E \to H \to M$ and $B \to D \to F \to J \to N$, respectively. By adopting the same analysis method for port 1 excitation, it can be deduced that

$$\begin{cases} \varphi_{32} = 135° \\ -\varphi_{32} - \theta_{23} = 135° \end{cases} \tag{2}$$

Similarly, for port 3 and port 4 excitation,

$$\begin{cases} -\varphi_{32} = -135° \\ \varphi_{32} + \theta_{32} = -135° \end{cases} \tag{3}$$

$$\begin{cases} \varphi_{23} = 45° \\ -\varphi_{23} + \theta_{32} = 45° \end{cases} \tag{4}$$

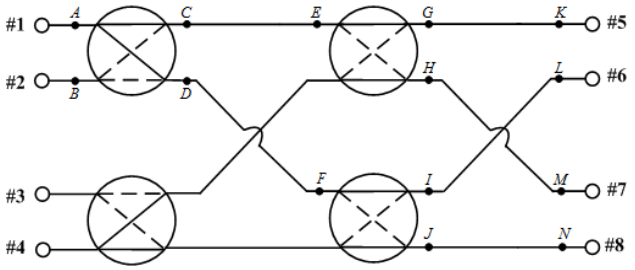

FIGURE 4. Signal meandering path to output ports when port 1 is fed.

After solving this set of equations, we can obtain

$$\begin{cases} \varphi_{23} = 45^\circ \\ \varphi_{32} = 135^\circ \\ \theta_{23} = 90^\circ \\ \theta_{32} = 90^\circ \end{cases} \tag{5}$$

It can be learnt from the calculated results that for type I hybrid coupler, 45° and 135° output phase differences are required when port 1 and port 4 are excited, respectively. While for type II hybrid coupler, based on the previous assumptions, it has equal output phase differences compared with 90° hybrid coupler. Hence, the type II modified hybrid coupler is actually a 90° hybrid coupler. For this reason, hereafter we refer the type I hybrid coupler as modified hybrid coupler and type II hybrid coupler as 90° hybrid coupler. Considering port 3 and port 4 excitations, the modified hybrid couplers near port 3 and port 4, shown in Fig. 4, must be mirrored with the modified hybrid coupler that neighbours port 1 and port 2. While for the two 90° hybrid couplers, they should be arranged in the same manner.

III. DESIGN PROCEDURE

From the previous discussions in Section II, two types of hybrid couplers are indispensable in design of the proposed Butler matrix: modified hybrid coupler and 90° hybrid coupler. The 90° hybrid coupler can be easily obtained and several implementations have been published in the literatures [17] and [18]. The modified hybrid coupler can be realized by 90° hybrid coupler cascaded with −45° phase to obtain 45° and 135° output phase differences at the same time. For each component, Rogers Duroid 5880 substrate with thickness of 0.508 mm, loss tangent of 0.0009 and relative dielectric permittivity of 2.2 is used. All the related components are implemented and optimized by applying the full-wave FEM simulation package, Ansoft HFSS ver. 15.

A. 90° HYBRID COUPLER

The topology of 90° hybrid coupler is shown in Fig. 5. Practically, SIW can be equivalent to the dielectric-filled rectangular waveguide as they have shown similar TE_{10}-like mode dispersion. In SIW structure, the narrow-walls are replaced by periodical metalized vias (0.4 mm diameter and 0.8 mm spacing in our design). For 90° hybrid

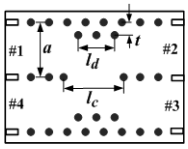

FIGURE 5. Topology of 90° SIW hybrid coupler.

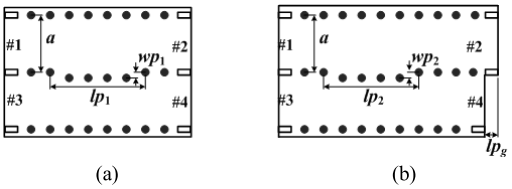

FIGURE 6. Configurations of (a) equal-length unequal-width phase shifter and (b) compensating phase shifter.

coupler, the required power splitting ratio and output phase difference can be achieved by adjusting the length and width of the coupling section. The dimension values of the structure are $a = 5$ mm, $ld = 4$ mm and $lc = 6.4$ mm. The performance of the 90° SIW hybrid coupler is given in Fig. 7. For port 1 excitation, the bandwidth of the 90° SIW hybrid coupler is larger than 13.3% for $S_{11} < -20$ dB. S_{41} is less than −20 dB over the whole operating band. Additionally, S_{21} and S_{31} are centred at −2.9 dB with a dispersion of ±0.2 dB, which means that the −3 dB power dividing between port 2 and port 3 is obtained approximately in the whole band. The simulated output phase difference is characterized by $\mathrm{Ang}(S_{21}) - \mathrm{Ang}(S_{31})$. The phase dispersion of 90° SIW hybrid coupler varies from 89.8° to 90.5° over the whole band. The simulated output phase difference agrees well with the ideal value. For port 4 excitation, the output phase difference is characterized by $\mathrm{Ang}(S_{34}) - \mathrm{Ang}(S_{24})$. Because of its symmetrical structure, the output phase difference of 90° SIW hybrid coupler is 90°, either port 1 or port 4 is fed. The crossover can be formed with two cascaded hybrid couplers and it has been validated by many designs [19]. Generally, a well-designed hybrid coupler will have good crossover performance.

B. MODIFIED HYBRID COUPLER

According to previous analyses, the modified hybrid coupler can be realized by 90° SIW hybrid coupler and −45° phase shifter. Since the 90° SIW hybrid coupler has been designed, the following steps are aimed to design a −45° phase shifter with good performance.

A SIW structure has different propagation constant with different SIW width. Generally, a wider SIW results in a larger propagation constant. However, as we know, the propagation constant grows in inverse proportion to the phase velocity which implies SIW width is inversely proportional to phase velocity as well. Thus, the equal length can obtain different phase shifting by varying the SIW width. This type of phase shifter is referred to as equal-length unequal width phase shifter, shown in Fig. 6(a). For SIW structure,

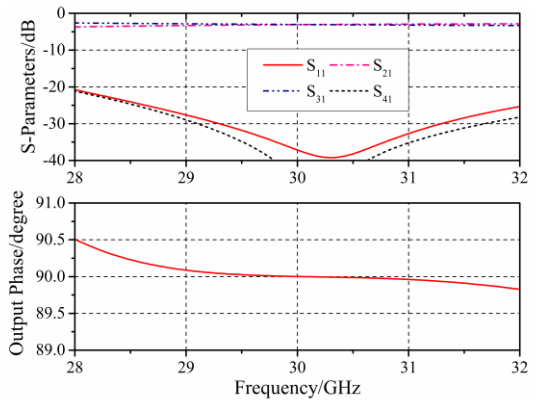

FIGURE 7. Simulated S-parameters of the 90° hybrid coupler and its output phase difference.

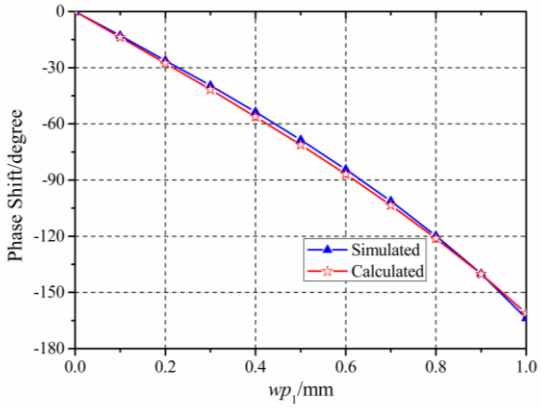

FIGURE 8. Relative phase difference with different values of wp_1@30GHz.

the propagation constant is dispersive and varies with frequency f. It can be written as (f: GHz, w: mm) [20]

$$\beta(f) = \sqrt{\left(\frac{2\pi\sqrt{\varepsilon_r}f}{300}\right)^2 - \left(\frac{\pi}{w}\right)^2} \tag{6}$$

where w is SIW width and ε_r is relative permittivity of the substrate. The phase shift $\varphi(f)$ is defined by

$$\varphi(f) = l\beta(f) \tag{7}$$

In (7), l is the wave travelling distance in SIW. For equal-length unequal-width phase shifter, its phase shift $\varphi(f)$ can be characterized by $\mathrm{Ang}(S_{21}) - \mathrm{Ang}(S_{43})$. Therefore, $\varphi(f)$ can be rewritten as

$$\varphi(f) = l\left[\sqrt{\left(\frac{2\pi\sqrt{\varepsilon_r}f}{300}\right)^2 - \left(\frac{\pi}{a - wp_1}\right)^2} - \sqrt{\left(\frac{2\pi\sqrt{\varepsilon_r}f}{300}\right)^2 - \left(\frac{\pi}{a + wp_1}\right)^2}\right] \tag{8}$$

Fig. 8 shows the simulated and calculated results. With wp_1 increasing, phase shifting decreases monotonously. The simulated and calculated results agree well with each other.

Another approach mostly used in phase shifter design is the delay line. Here, the compensating phase shifter combines the

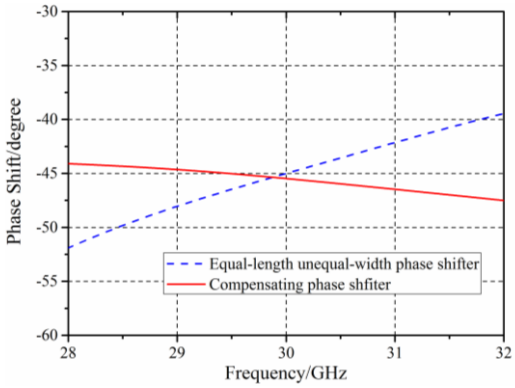

FIGURE 9. Phase shifts of equal-length unequal-width phase shifter and compensating phase shifter versus frequency.

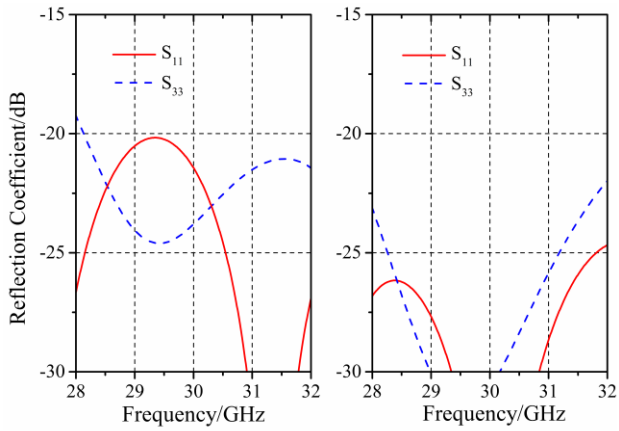

FIGURE 10. Reflection coefficient of (a) 45° equal-length unequal-width phase shifter and (b) 45° compensating phase shifter.

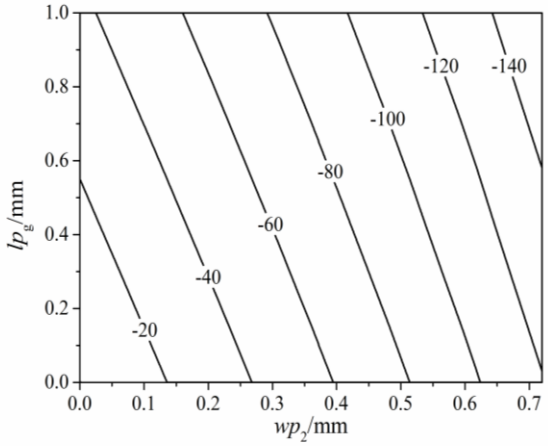

FIGURE 11. Phase shift of compensating phase shifter versus wp_2 and lp_g@30GHz.

characteristics of equal-length unequal-width phase shifter with a delay line, shown in Fig. 6(b). The phase shift at the centre frequency f_0 can be expressed with the following formula

$$\varphi(f_0) = lp_2\beta_2 - lp_g\beta_3 - lp_2\beta_1 = lp_2(\beta_2 - \beta_1) - lp_g\beta_3 \tag{9}$$

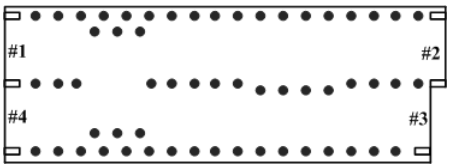

FIGURE 12. Topology of the modified hybrid coupler.

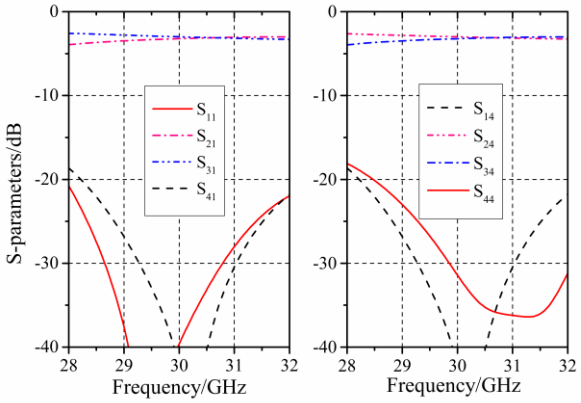

FIGURE 13. Simulated S-parameters of the modified hybrid coupler.

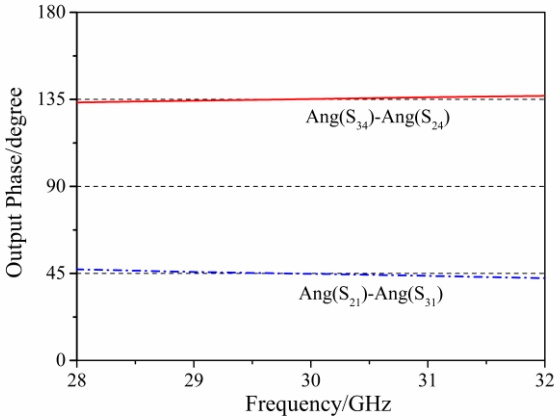

FIGURE 14. Output phase differences of the modified hybrid coupler.

where in β_1, w equals $a-wp_2$; in β_2, w is the same as $a+wp_2$, and in β_3, w equals a. For comparison, the phase characteristic and reflection coefficients of equal-length unequal-width phase shifter and compensating phase shifter are given in Fig. 9 and Fig. 10. As shown in Fig. 9, the phase error of equal-length unequal-width phase shifter is within 12° in the whole band. While for the compensating phase shifter, the phase error is only within 3° over the band. The compensating phase shifter provides better phase performance in the operating bandwidth. Hence, it will be adopted in the following design of the modified hybrid coupler. The values of a, lp_1, wp_1, wp_2, lp_g are 5 mm, 8.8 mm, 0.34 mm, 0.12 mm and 0.8 mm, respectively. Fig. 11 shows the phase shift of the compensating phase shifter versus wp_2 and lp_g at 30 GHz. It can be learnt that the larger wp_2 and lp_g will lead to a larger phase delay.

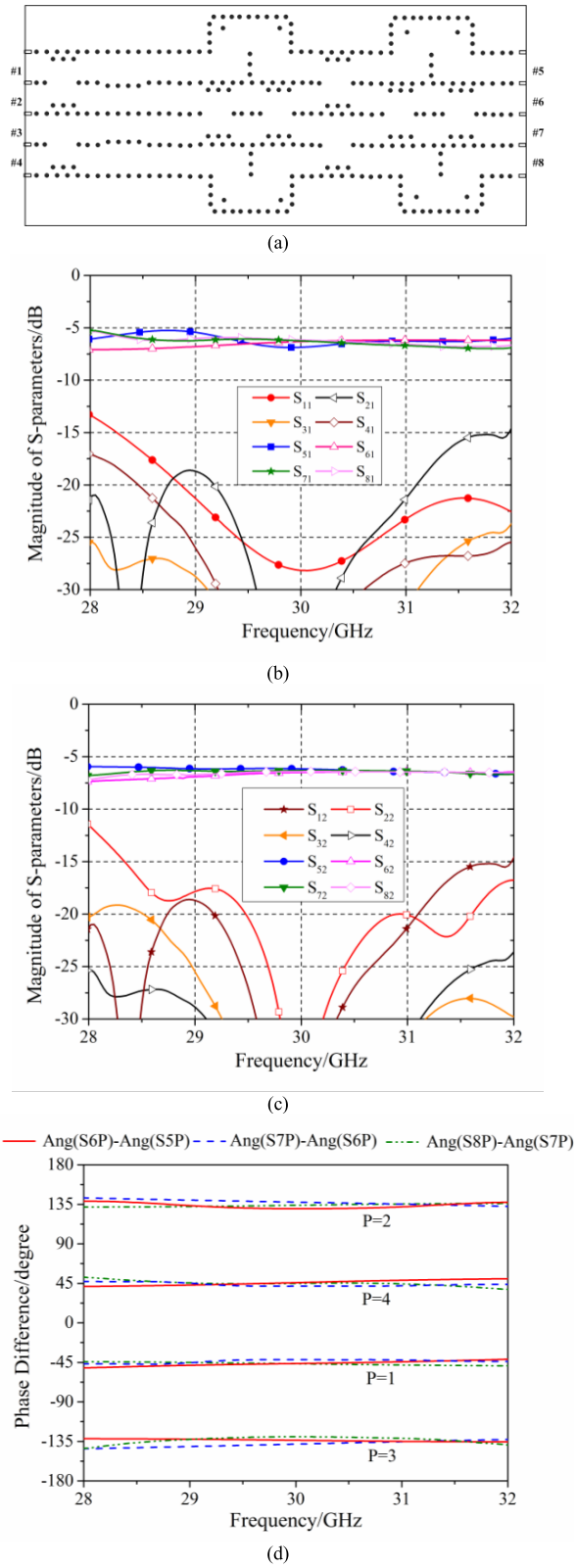

FIGURE 15. (a) Geometry of the proposed SIW Butler matrix. (b) simulated magnitude of S-parameters with port 1 excitation. (c) simulated magnitude of S-parameters with port 2 excitation. (d) output phase differences of Butler matrix. Here, P is the input port number.

By combining the designed 90° SIW hybrid coupler with the −45° compensating phase shifter, one can obtain the

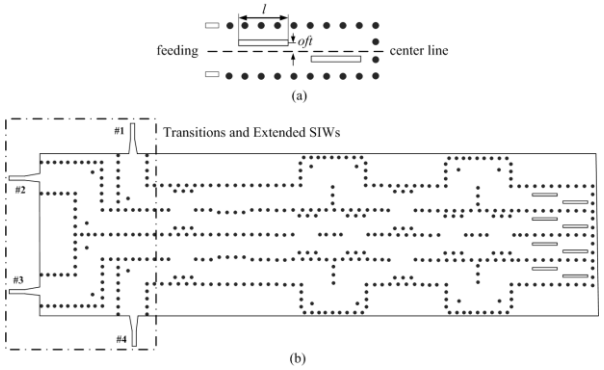

FIGURE 16. (a) Geometry of the branch SIW slot antennas. (b) demonstration of the SIW multibeam slot antenna array.

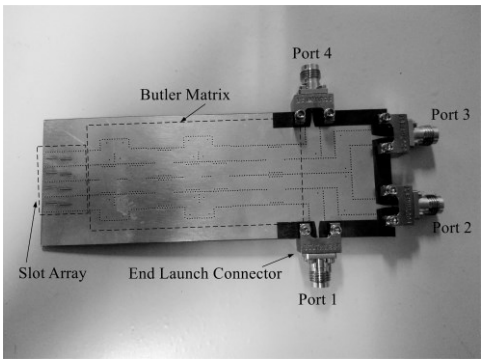

FIGURE 17. Photograph of the fabricated SIW multibeam array.

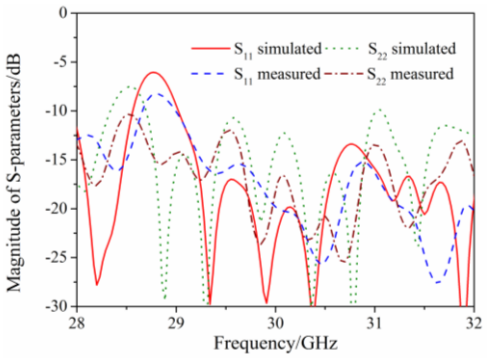

FIGURE 18. Simulated and measured reflection coefficients.

modified hybrid phase shifter, shown in Fig. 12. For port 1 or port 4 excitation, as shown in Fig. 13, the ±0.2dB power equality bandwidth is 9.3%, from 29.2 GHz to 32 GHz. The return loss ($-S_{11}$ and $-S_{44}$) is better than 18.8 dB and isolation is above 18.9 dB in the whole band. Fig. 14 represents the relative output phase differences of the modified hybrid coupler. As shown in this figure, the phase differences are 135° ± 1.8° and 45° ± 1.8° in the whole band. Thus, the −45° compensating phase shifter keeps the good performance of hybrid coupler and the design purpose of the modified hybrid coupler with both 45° and 135° output phase differences is reached.

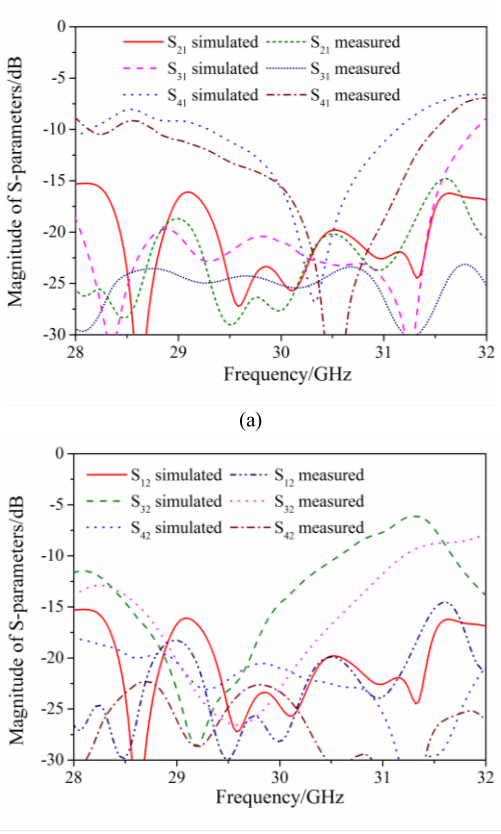

FIGURE 19. Simulated and measured coupling coefficients. (a) port 1 excitation. (b) port 2 excitation.

C. CASCADED SIMULATION

The geometry of the proposed Butler matrix is shown in Fig. 15 (a). Fig. 15 (b)−(d) presents the simulated magnitude of S-parameters and output phase differences, respectively. For port 1 and port 2 excitation, coupling to the output ports is well equalized at −6.3 dB with 1.2 dB dispersion across the entire operating bandwidth of interest from 28 GHz to 32 GHz. Actually, the 0.3 dB loss is related to the loss tangent of 0.0009 given by the manufacturer. The reflection coefficient at port 1 and port 2, and the coupling level of the two ports to the other input ports are almost better than −12 dB over the entire bandwidth. The phase dispersions are with peak to peak error of 13°, near the theoretical values of −45°, 135°, −135°, and 45°, respectively.

IV. ANTENNA ARRAY AND MEASUREMENTS

For its excellent polarization purity and low profile, slot antenna arrays have been widely used in mmWave applications. The detailed geometry of slot element is shown in Fig. 16(a). The element spacing is 4.95 mm ($0.495\lambda_0$@30 GHz) and each branch consists of two identical and staggered slot elements. The slot length and its offset from the centre line are $l = 4.08$ mm and $oft = 0.32$ mm, respectively. To validate the design, the whole geometry, also including the transitions and extended SIWs,

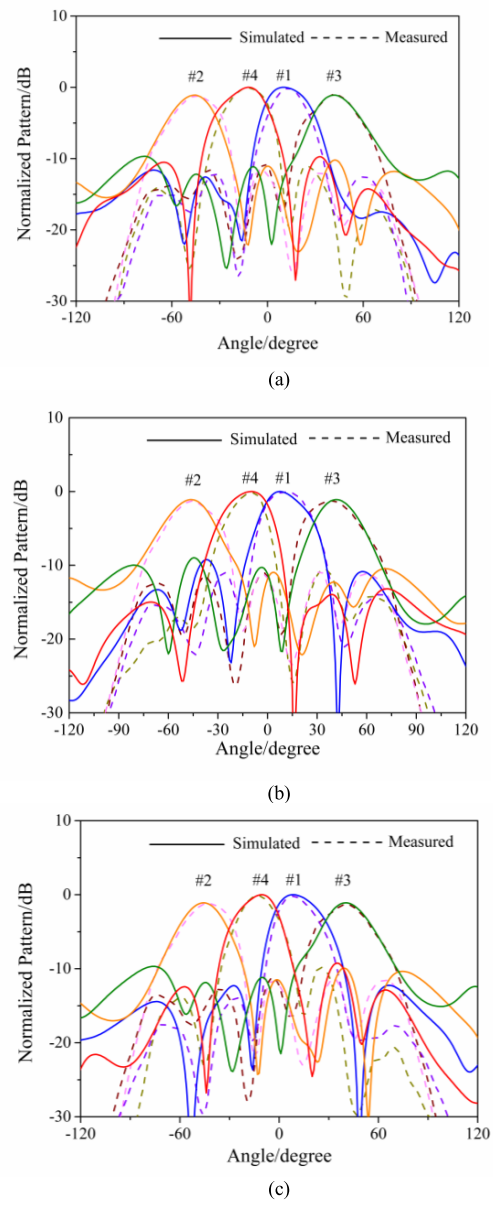

FIGURE 20. Simulated and measured radiation patterns of the multibeam antenna array. (a) $f = 29.5$ GHz. (b) $f = 30$ GHz. (c) $f = 30.5$ GHz.

is illustrated in Fig. 16(b). The whole circuit was implemented on Rogers 5880 dielectric substrate, as shown in Fig. 17. The measurements of S-parameters, radiation patterns and gain were accomplished using Agilent E8363B Vector Network Analyzer, and a far-field anechoic chamber system. Except for the port under test, the other ports are terminated with 50Ω broadband matching loads through 2.40 mm end launch connectors. The overall dimension of this prototype is 110.28×42.5 mm^2.

A. RETURN LOSS AND ISOLATION

The return losses and coupling coefficients between two input ports were measured over 28 GHz to 32 GHz. The measured return loss of port 1 is better than 10 dB over whole bandwidth

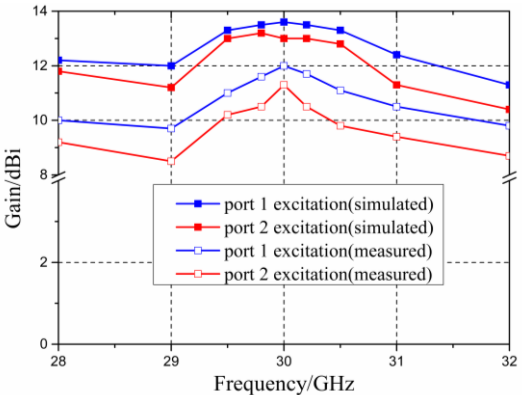

FIGURE 21. Simulated and measured gain of the antenna array.

except the range 28.7 GHz to 29 GHz, shown in Fig. 18. For port 2, return loss greater than 10 dB is able to cover the entire bandwidth, even though the simulated return loss is less than 10 dB in the range from 28.5 GHz to 28.8 GHz. The difference is caused by the dielectric loss which underestimated the loss factor in simulation. Additionally, it can be noted that the coupling coefficient between port 1 and port 4 is greater than −10 dB at some frequencies, shown in Fig. 19. In the higher frequency range, the coupling between port 2 and port 3 is greater than −10 dB, too. These phenomena can be attributed to the considerable mutual couplings between the adjacent branches of slot element and part of them (mutual couplings) flowing back to the input ports. For the identical polarization of each slot element and very close distance ($0.5\lambda_0$@ 30 GHz) between two branches, it is quite difficult to decrease the mutual coupling in such a slot array. The use of EBG structure can be considered to address this problem.

B. RADIATION PATTERN AND GAIN

The radiation patterns were tested at different frequencies. The four beams can realize a wide azimuthal coverage between ±61°. The shape and pointing angle of each radiation beam can be maintained over 29.5 GHz to 30.5 GHz, shown in Fig. 20. The pointing angles are 12° (port 1), −51° (port 2),51° (port 3), −12° (port 4), while the theoretical calculations are 13.8° (port 1), −48.2° (port 2), 48.2° (port 3) and −13.8° (port 4). The maximum side lobe level is −8.5 dB which is higher than the optimum −13 dB in theory. It is primarily caused by the sizable ground plane of Butler matrix itself.

Fig. 21 represents the simulated and measured gain of the antenna array when ports 1 ∼ 2 are excited, respectively. The gain of the other ports should be similar because of the symmetrical geometry of the design. The measured frequencies were 28 GHz, 29 GHz, 29.5 GHz, 29.8 GHz, 30 GHz, 30.2 GHz, 30.5 GHz, 30.8 GHz, 31 GHz and 32 GHz. Excited at port 1, the measured gain is in the range of 9.7 ∼ 12 dBi. The maximum gain is measured to be 12 dBi at 30 GHz while the minimum is 9.7 dBi at 29 GHz. However, the measured gains are less than the simulated counterparts by an average

of 2 dB, which may be caused by the additional insertion loss of the extended SIWs and the Butler matrix. For port 2 excitation, similar results can be obtained, shown in Fig. 21.

V. CONCLUSION

In this paper, a Butler matrix with modified hybrid coupler has been studied. The modified hybrid coupler is capable of outputting 45°/135° phase differences and exhibits excellent performance with wideband and flat phase balance, $135° \pm 1.8°$ and $45° \pm 1.8°$ in the whole operating band. This type of coupler dramatically facilitates the design flexibility of Butler matrix. Phase dispersions of the designed Butler matrix are with peak to peak error of 13°. The slot array fed by the designed Butler matrix can radiate four slanted beams with acceptable measured gain, in the range of $9.7 \sim 12$ dBi for port 1 excitation and $8.4 \sim 11.1$ dBi for port 2 excitation. The four beams can reach a wide azimuthal coverage between $\pm 61°$. With advantages of more flexibility in design, simple structure and good radiating performance, the Butler matrix with modified hybrid coupler would be an attractive candidate in 5G mmWave communications.

REFERENCES

[1] Y. J. Cheng *et al.*, "Substrate integrated waveguide (SIW) rotman lens and its Ka-band multibeam array antenna applications," *IEEE Trans. Antennas Propag.*, vol. 56, no. 8, pp. 2504–2513, Aug. 2008.

[2] T. Djerafi and K. Wu, "A low-cost wideband 77-GHz planar Butler matrix in SIW technology," *IEEE Trans. Antennas Propag.*, vol. 60, no. 10, pp. 4949–4954, Oct. 2012.

[3] Y. Li and K. M. Luk, "A multibeam end-fire magnetoelectric dipole antenna array for millimeter-wave applications," *IEEE Trans. Antennas Propag.*, vol. 64, no. 7, pp. 2894–2904, Jul. 2016.

[4] Y. J. Cheng and Y. Fan, "Millimeter-wave miniaturized substrate integrated multibeam antenna," *IEEE Trans. Antennas Propag.*, vol. 59, pp. 4840–4844, Dec. 2011.

[5] A. B. Guntupalli, T. Djerafi, and K. Wu, "Two-dimensional scanning antenna array driven by integrated waveguide phase shifter," *IEEE Trans. Antennas Propag.*, vol. 62, no. 3, pp. 1117–1124, Mar. 2014.

[6] K. Tekkouk, J. Hirokawa, R. Sauleau, M. Ettorre, M. Sano, and M. Ando, "Dual-layer ridged waveguide slot array fed by a Butler matrix with sidelobe control in the 60-GHz band," *IEEE Trans. Antennas Propag.*, vol. 63, no. 9, pp. 3857–3867, Sep. 2015.

[7] T. Djerafi, N. J. G. Fonseca, and K. Wu, "Broadband substrate integrated waveguide 4×4 Nolen matrix based on coupler delay compensation," *IEEE Trans. Microw. Theory Techn.*, vol. 59, no. 7, pp. 1740–1745, Jul. 2011.

[8] T.-Y. Chin, J.-C. Wu, S.-F. Chang, and C.-C. Chang, "A V-band 8×8 CMOS Butler matrix MMIC," *IEEE Trans. Microw. Theory Techn.*, vol. 58, no. 12, pp. 3538–3546, Dec. 2010.

[9] Y. J. Cheng, X. Y. Bao, and Y. X. Guo, "60-GHz LTCC miniaturized substrate integrated multibeam array antenna with multiple polarizations," *IEEE Trans. Antennas Propag.*, vol. 61, no. 12, pp. 5958–5967, Dec. 2013.

[10] Y. Y. Yang, W. Q. Che, W. C. Yang, and C. Fan, "Millimeter-wave multibeam antenna based on 2-D SIW beam-scanning network," in *Proc. Int. Workshop Electromagn. Appl. Student Innov. Competition (iWEM)*, Dec. 2015, pp. 1–2.

[11] A. A. M. Ali, N. J. G. Fonseca, F. Coccetti, and H. Aubert, "Design and implementation of two-layer compact wideband Butler matrices in SIW technology for Ku-band applications," *IEEE Antennas Propag. Mag.*, vol. 59, no. 2, pp. 503–512, Jan. 2010.

[12] S. Karamzadeh, V. Rafii, M. Kartal, and B. S. Virdee, "Compact and broadband 4×4 SIW Butler matrix with phase and magnitude error reduction," *IEEE Antennas Wireless Propag. Lett.*, vol. 25, no. 12, pp. 772–774, Dec. 2015.

[13] Y. J. Cheng, W. Hong, and K. Wu, "Millimeter-wave multibeam antenna based on eight-port hybrid," *IEEE Microw. Wireless Compon. Lett.*, vol. 19, no. 4, pp. 212–214, Apr. 2009.

[14] Q. L. Yang, Y. L. Ban, K. Kang, C. Y. D. Sim, and G. Wu, "SIW multibeam array for 5G mobile devices," *IEEE Access*, vol. 4, pp. 2788–2796, Jun. 2016.

[15] B. Liu, W. Hong, Z. C. Hao, and K. Wu, "Substrate integrated waveguide 180-degree narrow-wall directional coupler," in *Proc. Asia–Pacific Microw. Conf. (APMC)*, Suzhou, China, vol. 1. Dec. 2005, pp. 559–561.

[16] Y. J. Cheng, W. Hong, and K. Wu, "Novel substrate integrated waveguide fixed phase shifter for 180-degree directional coupler," in *IEEE MTT-S Int. Microw. Symp. Dig.*, Honolulu, HI, USA, Jun. 2007, pp. 189–192.

[17] Z. C. Hao, W. Hong, J. X. Chen, H. X. Zhou, and K. Wu, "Single-layer substrate integrated waveguide directional couplers," *IEE Proc.-Microw. Antennas Propag.*, vol. 153, no. 5, pp. 426–431, Oct. 2006.

[18] F. Carrera, D. Navarro, M. Baquero-Escudero, V. M. Rodrigo-Peñarrocha, "Compact substrate integrated waveguide directional couplers in Ku and K bands," in *Proc. 40th Eur. Microw. Conf.*, Paris, France, Sep. 2010, pp. 1178–1181.

[19] C. Collado, A. Grau, and F. De Flaviis, "Dual-band Butler matrix for WLAN systems," in *IEEE MTT-S Int. Microw. Symp. Dig.*, Jun. 2005, pp. 2247–2250.

[20] Y. J. Cheng, W. Hong, and K. Wu, "Broadband self-compensating phase shifter combining delay line and equal-length unequal-width phaser," *IEEE Trans. Microw. Theory Techn.*, vol. 58, no. 1, pp. 203–210, Jan. 2010.

QING-LING YANG was born in Jiangxi, China, in 1989. He received the B.S. degree from the Chengdu University of Information Technology in 2014, where he is currently pursuing the master's degree from the School of Electronic Engineering, University of Electronic Science and Technology of China, Chengdu. His main research interests are millimeter wave multibeam antenna array with Butler matrix and Rotman lens for 5G wireless communications.

YONG-LING BAN was born in Henan, China, in 1978. He received the B.S. degree in mathematics from Shandong University, the M.S. degree in electromagnetics from Peking University, and the Ph.D. degree in microwave engineering from the University of Electronic Science and Technology of China (UESTC), in 2000, 2003, and 2006, respectively. In 2006, he joined the Xi'an Mechanical and Electric Information Institute as a Microwave Engineer. He then joined Huawei Technologies Co., Ltd., Shenzhen, China, first as an RF Antenna Design Engineer and then as a Senior Design Engineer. At Huawei, he designed and implemented various terminal antennas for 15 data card and mobile phone products customized from leading telecommunication industries like Vodafone. Since 2010, he has been with UESTC as an Associate Professor of Microwave Engineering, where he is currently a Professor. From 2014 to 2015, he visited the Queen Mary University of London as a Visiting Scholar. He has authored over 60 referred journal and conference papers on these topics. He holds over 20 granted and pending Chinese and overseas patents. His research interests include wideband small antennas for 4G/5G handset devices, MIMO antenna, and millimeter wave antenna array.

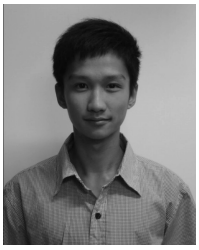

JI-WEI LIAN was born in Guangdong, China, in 1992. He received the B.S. degree in electronics science and technology from Hunan University, Hunan, China, in 2015. He is currently pursuing the master's degree in electromagnetic field and microwave technology with the University of Electronic Science and Technology of China, Chengdu, China. His current research interests include millimeter-wave antennas and arrays for millimeter-wave applications.

ZHE-FENG YU was born in Jilin, China. He received the M.S. degree in aerodynamics from the China Aerodynamics Research and Development Center (CARDC) in 2002, and the Ph.D. degree in electromagnetics from Peking University, in 2005. In 1999, he joined CARDC as a Microwave Engineer, where since 2015, he has been a Professor of Microwave Engineering. From 2004 to 2005 and from 2014 to 2015, he visited Lomonosov Moscow State University and the University of Cambridge as a Scholar Visitor, respectively. He has authored over 40 referred journal and conference papers on these topics. His research interests include wideband small antennas for 4G/5G handset devices, millimeter wave, and reentry blackout.

BIAN WU was born in Hubei, China, in 1981. He received the B.Eng. degree in electronic and information engineering and the Ph.D. degree in electromagnetic and microwave technology from Xidian University, Xi'an, China, in 2004 and 2008, respectively. In 2008, he joined the School of Electronic Engineering, Xidian University. In 2013, he was a Post-Doctoral Visitor with the Queen Mary University of London, U.K. He is currently a Professor with the National Key Laboratory of Antennas and Microwave Technology. His research interests include microwave circuits and devices, graphene-based metamaterials, antennas and wireless sensors.